

Al-dependent electronic and magnetic properties of YCrO_3 with magnetocaloric application: an ab-initio and Monte- Carlo approach

Tushar Kanti Bhowmik^{a,*}, Tripurari Prasad Sinha^a

^aBose Institute, Department of Physics, 93/1, APC Road, Kolkata- 700009, India

ARTICLE INFO

Keywords:

Perovskite
DFT
Monte-Carlo Simulation
Critical Temperature
Magnetocaloric effect
RCP

ABSTRACT

In this paper, a theoretical journey from electronic to magneto-caloric effect has been shown through the magnetic properties of aluminium induced yttrium chromate. The ground state electronic band structure and density of states have been studied using first principle calculations under GGA+U schemes. From the energy minimization, the ferromagnetic structure is more stable than the anti-ferromagnetic one. The interaction constant as well as the magnetic moment, have been determined from mean-field theory and DFT, respectively. The Monte-Carlo simulation under Metropolis algorithm has been employed to determine the critical temperature (T_C), which is nearly same as the experimental value. The temperature-dependent magnetization shows that these materials exhibit a paramagnetic to ferromagnetic phase transition at 136 K, 130 K, 110 K, and 75 K respectively. The two inherent properties named the isothermal entropy change (ΔS_M) and the adiabatic temperature change (ΔT_{ad}) as a function of temperature for different applied magnetic fields have been determined to measure the magnetocaloric efficiency of these materials. The relative cooling power (RCP), which is calculated around T_C , changes from 4.7 J/Kg to 2.5 J/Kg with the decreasing Cr- concentration.

1. Introduction

The ferromagnetic insulators [1–4] as well as semiconductors [5–8] within the group of perovskites have been drawing the tremendous interest in material research since last few decades due to their multi-functional properties such as magneto-capacitance [9, 10], magneto-dielectric [11, 12], magneto-resistance [13, 14], magnetocaloric effect (MCE) [15, 16] etc. They have been applied in various fields such as spintronics [17], opto-electronics [18], piezoelectric [19]. However, we have focused on the magnetocaloric material, which is used in the magnetic refrigeration for cooling at room temperature as well as the cryogenic application [20, 21]. In the common refrigerator the cooling is done by compressing the vapour cycle [22], which is very harmful for environment. But in magnetic refrigerator it is accomplished by application or removal of external magnetic field, which induces the magneto-caloric effect in these materials [23]. The adiabatic temperature change (ΔT_{ad}) and the isothermal magnetic entropy change (ΔS_m), which are the intrinsic properties of the material, are the two important factors for the MCE. The magnetic refrigerator needs the magnetic materials, whose critical temperature (T_C) have within the range of requiring cooling temperature. So, we have been searching for the low cost magnetic perovskites, which have large MCE at transition temperature and provides the better degree of efficiency without affecting the environment.

To know the underlying physics behind these strongly correlated materials, the density functional theory (DFT) [24] is beneficial and accurate until now. Using generalised gradient approximation (GGA) method [25] it can predict various properties of matter. It can be accurately described the d and f- electrons of strongly correlated systems by adding

the Coulomb potential (U) with DFT (DFT+U) [26]. But this theory can not count the thermal fluctuations present in the system. But, it is necessary to discuss the temperature-dependent behaviour of this type of material. In the critical region, where the phase transition occurs, the DFT can not explain the physics behind it. There are several types of theoretical models such as mean-field theory [27], 3D- Heisenberg model [28], 3D Ising model [29], etc., to describe this behaviour accurately. These models are enabled to explain the mechanism near phase transition and help us to find the appropriate materials for MCE. Usually, the Monte-Carlo simulation technique has been used to describe these models [30].

In this context, we have targeted to reach the liquid nitrogen temperature (77 K), so that we can easily replace liquid nitrogen as a frigging element, which is very costly and uneasy to handle. So, we use the yttrium chromate (YCrO_3) ($T_C = 140$ K) [31] as a starting material and then we doped a non-magnetic aluminium (Al) to Cr site to decrease the critical temperature. With 50% doping of Al [32], we have achieved that the T_C is 73 K. At first, we have used DFT to know the Fermi energy, the density of states (DOS), bandgap energy. We have studied the band structure and DOS of 10% and 30% doping of Al with full potential linear augmented plane wave (FPLAPW) method [33]. From DFT, we can easily predict the ground state magnetic configuration of these materials. After that, we have used the Ising model to determine the transition temperatures (T_C), magnetic susceptibility (χ), and hysteresis loop with the help of Metropolis Monte- Carlo algorithm. At last, we have calculated the adiabatic temperature change (ΔT_{ad}) as well as the relative cooling power (RCP) to determine the magnetocaloric efficiency of these systems.

*Corresponding author

✉ tkb746@gmail.com (T.K. Bhowmik)
ORCID(s):

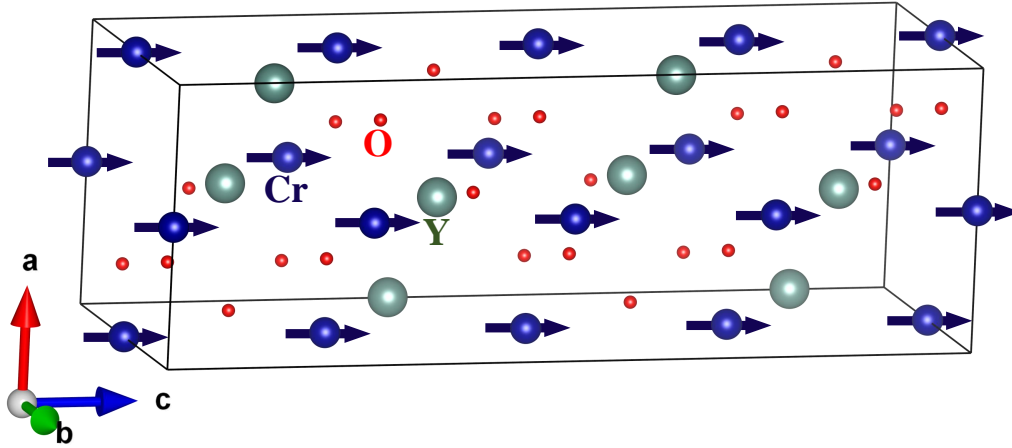


Figure 1: Crystal structure of YCrO_3 , used for theoretical calculations and the blue arrows signify the spin direction of Cr-atom with FM configuration.

2. Computational Details

2.1. Ab-initio Calculations

Density functional theory (DFT) is implemented to study the electronic structure and magnetic properties of Al-doped YCrO_3 . The full-potential linearized augmented plane wave (FP-LAPW) method has been used to solve the Kohn-Sham equations as implemented in WIEN2K package [34, 35]. The general gradient approximation (GGA) with Coulomb repulsion U (GGA+ U) method has been employed to optimize the crystal structures as well as determining the electronic structure and the magnetic moment calculations. We have used different supercell of 40 atoms with P1 spacegroup and replaced the Cr atom with Al atom appropriately to construct the $\text{YAl}_{0.1}\text{Cr}_{0.9}\text{O}_3$ and $\text{YAl}_{0.3}\text{Cr}_{0.7}\text{O}_3$ structures. The muffin-tin radii (R_{mt}) for Y, Al, Cr and O atoms are 2.26 Å, 1.89 Å, 1.78 Å and 1.69 Å respectively. The cut-off energy ($R_{mt} \times K_{max}$) from core states to valence states has been set to 6 eV. 500 k-points have been used in the whole Brillouin zone for self-consistent convergence. The Hubbard parameter $U_{eff} = U - J = 4$ eV have been used for Cr-3d states. The energy convergence criteria are set to 10^{-4} Ry, whereas the charge convergence is fixed to 10^{-3} e for self-consistent optimization calculations of Al-doped YCrO_3 .

The electronic structure of Al-doped YCrO_3 has been calculated using the GGA+ U method. It is reported that YCrO_3 crystallizes with the orthorhombic Pnma space group. In the case of Al-doped YCrO_3 , the supercell has been generated in WIEN2k struct file and replaced the Chromium with Aluminium appropriately to maintain the doping concentration. The spin direction of the magnetic Cr-ions are set to the upward direction for FM calculations. In order to see the magnetic structure, we have tried with AFM spin configuration between Cr-ions also. According to the energy value of these FM and AFM configurations, we have seen

the FM-spin obtained the minimal energy value for all cases. The detailed magnetic properties have been described in the following sections. The calculated structure has been optimized according to WIEN2k spin-polarized algorithm. After that, the density of states and band structure have been calculated.

2.2. Monte-Carlo Simulations

Yttrium Chromate (YCO) is a single perovskite ABO_3 like structure where A site cation Y^{3+} is non magnetic but B site cation Cr^{3+} is a magnetic one. So we have considered the magnetic interaction between Cr^{3+} - Cr^{3+} ions only. The other three samples we have doped randomly the non magnetic Al^{3+} ions in different ratios in Cr-site. The interaction constant between Cr^{3+} and Al^{3+} is taken to zero due to the non magnetic Al^{3+} ion. So we have considered only Cr^{3+} - Cr^{3+} nearest neighbour (nn) and next nearest neighbour (nnn) interaction here. We have taken Ising model Hamiltonian with nn and nnn for the simulation.

$$H = -J_1 \sum_{\langle i,j \rangle} s_i s_j - J_2 \sum_{\langle\langle i,k \rangle\rangle} s_i s_k - h \sum_i s_i \quad (1)$$

Where J_1 and J_2 are the nn and nnn interaction constants and $\langle i, j \rangle$ and $\langle\langle i, k \rangle\rangle$ are nn and nnn sites respectively. From previous experimental study of YCO, we have seen that it crystallizes with orthorhombic Pnma space group where the Cr^{3+} ion forms CrO_6 octahedra with all six nearest O^{2-} ions. The antiferromagnetic ordering temperature is $T_N = 140$ K but below ordering temperature hysteresis curve have been shown that there was some weak ferromagnetism present in this material. In our magnetic monte carlo simulation study, we have considered only magnetic Cr^{3+} ion, which positioned at the corner of the cubic crystal structure and nn interaction between two Cr- ion have chosen to anti-

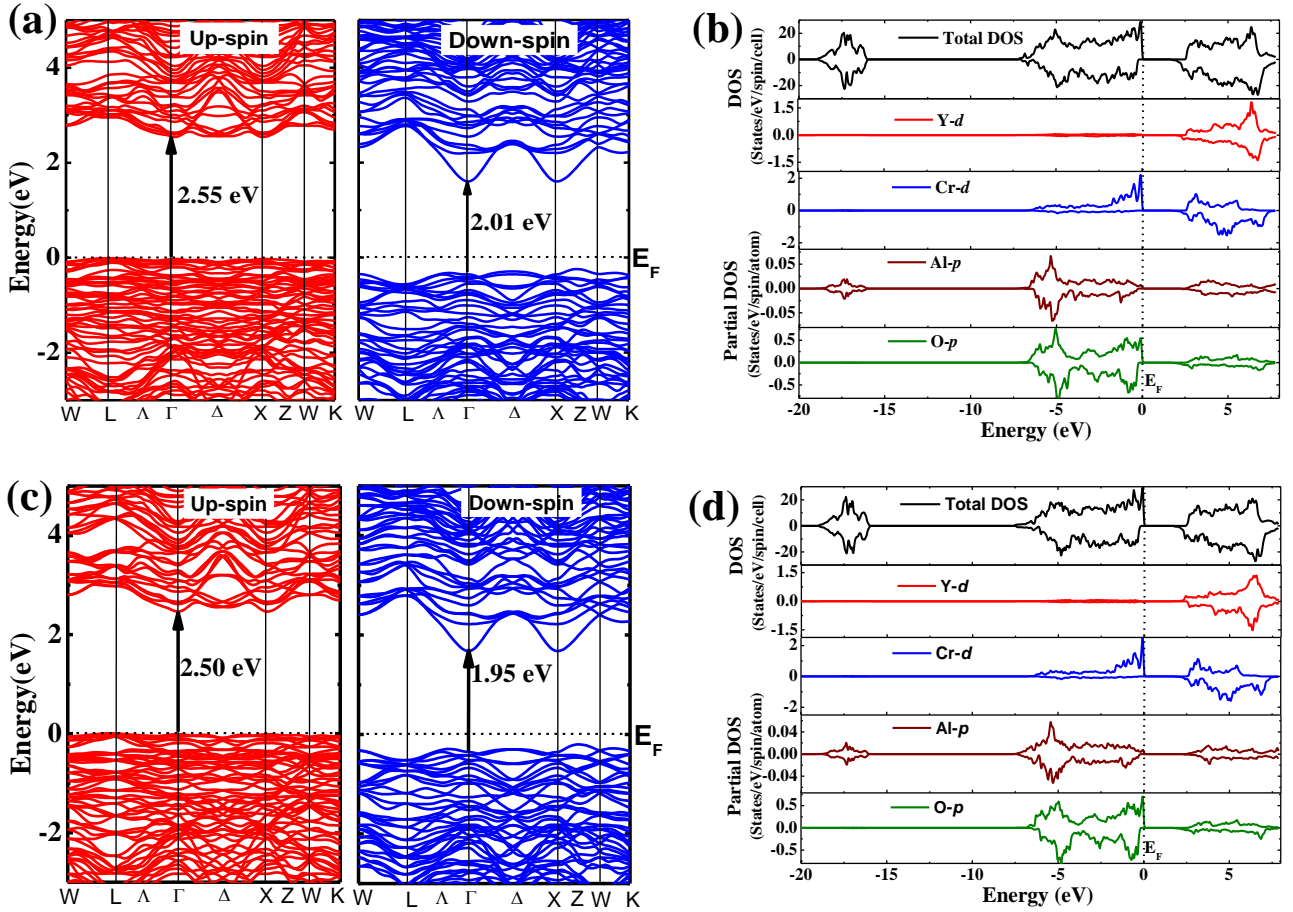


Figure 2: Band structure from GGA+U method for up spin (red) and down spin (blue) configuration for (a) $\text{YCr}_{0.9}\text{Al}_{0.1}\text{O}_3$ (c) $\text{YCr}_{0.7}\text{Al}_{0.3}\text{O}_3$. Density of states (DOS) and Partial DOS for different atoms for (b) $\text{YCr}_{0.9}\text{Al}_{0.1}\text{O}_3$ (d) $\text{YCr}_{0.7}\text{Al}_{0.3}\text{O}_3$

ferromagnetic whereas nnn interaction is considered to be antiferromagnetic. We have used the mean field approximation [36] to determine the interaction constants J_1 (nn) and J_2 (nnn).

$$T_N = \frac{2}{3k_B} ZS(S+1)J_{eff} \quad (2)$$

The value of the transition temperatures ($T_N = 140$ K) are taken from the previous experimental study and Z are the coordination number (Here $Z = 6$ and $S = 3/2$). The values of J_{eff} , which have been calculated from equation (2), are 9.33 K, 9.85 K, 12.78 K and 13.9 K for YCrO_3 , $\text{YAl}_{0.1}\text{Cr}_{0.9}\text{O}_3$, $\text{YAl}_{0.3}\text{Cr}_{0.7}\text{O}_3$ and $\text{YAl}_{0.5}\text{Cr}_{0.5}\text{O}_3$ respectively.

We have done Monte-Carlo simulation (MCS) using the Metropolis algorithm to determine the magnetic properties of $\text{YAl}_x\text{Cr}_{1-x}\text{O}_3$ ($x = 0, 0.1, 0.3, 0.5$). In the MCS process, the periodic boundary condition and standard sampling method have been applied over the whole lattice of size $L = 30$ in all three Cartesian directions. Single flip metropolis algorithm has been used to solve the above Ising Hamiltonian, described at equ (1). If the change in energy (dE) is less than zero, or the transition probability [$\exp(-dE/k_B T)$] is

greater than a random value, the flip is accepted otherwise rejected. 10^6 MCS steps have been used to reach the equilibrium of lattices and next 10^7 steps to average the magnetization and other observables. The physical quantities, which have been measured using MCS, are described as follows. The internal energy per site is,

$$E = \frac{1}{N} \langle H \rangle \quad (3)$$

Where $N = L \times L \times L$ is the total number of lattice points. The magnetisation of Cr^{3+} ions in these materials is,

$$M = \langle \frac{1}{N} \sum_i S_i \rangle \quad (4)$$

The magnetic susceptibility is given by,

$$\chi = \frac{\langle M^2 \rangle - \langle M \rangle^2}{k_B T} \quad (5)$$

The magnetic specific heat is calculated by,

$$C_m = \frac{\langle E^2 \rangle - \langle E \rangle^2}{k_B T^2} \quad (6)$$

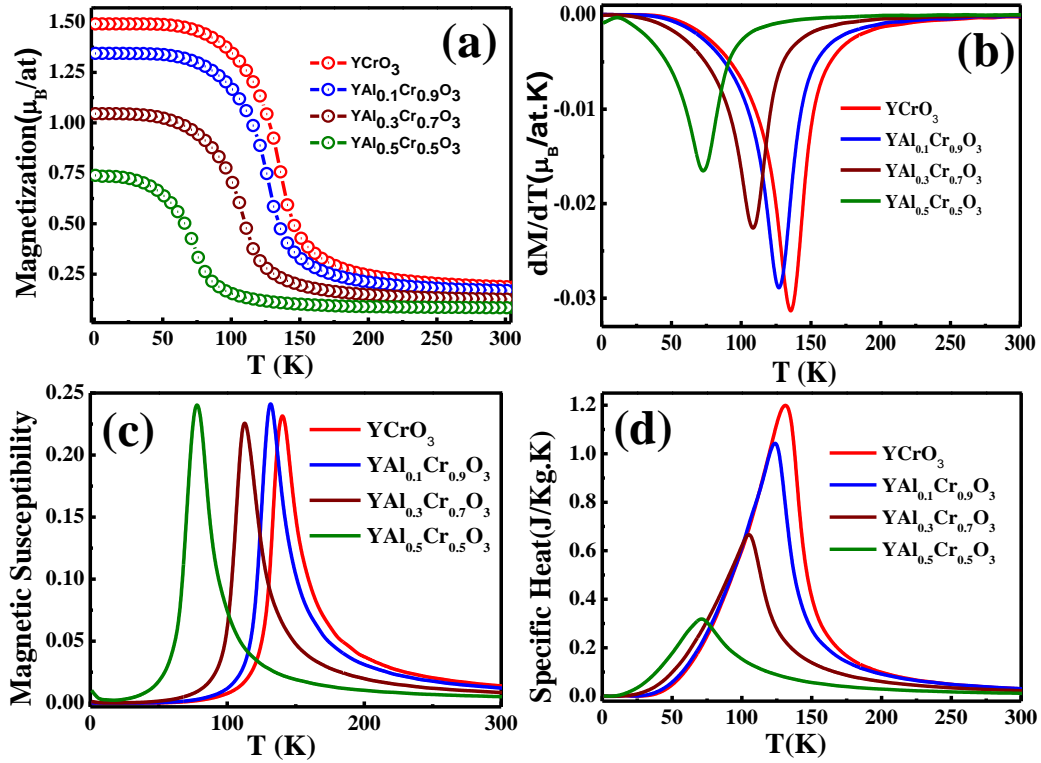


Figure 3: (a) Temperature dependent magnetization for different Al doping concentration. (b) 1st derivative of M vs T curves for all materials. (c) Magnetic susceptibility vs temperature curves and (d) Specific heat with respect to temperature for $\text{YCr}_{1-x}\text{Al}_x\text{O}_3$.

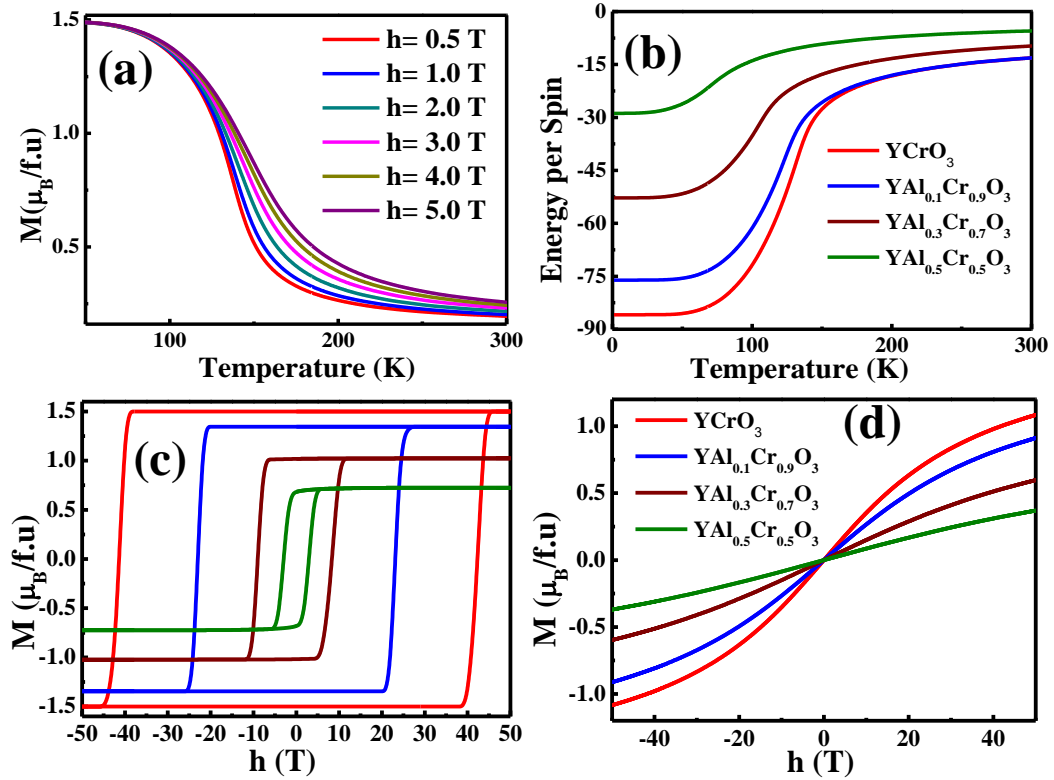


Figure 4: (a) Magnetization versus temperature at different external field for YCrO_3 . (b) Temperature dependency of energy per spin of different samples. (c) M-H loop at 20 K. (d) M-H curve at room temperature for different materials.

The magnetic entropy is given by

$$S_m = \int_0^T \frac{C_m}{T} dT \quad (7)$$

The change in magnetic entropy is described as

$$\Delta S_m = \int_0^{h_{max}} \left(\frac{\partial M}{\partial T} \right) dh \quad (8)$$

Where h_{max} is the maximum applied field and $\left(\frac{\partial M}{\partial T} \right)_h$ is the thermal magnetisation for a fixed external magnetic field h . The adiabatic temperature change is given by

$$\Delta T_{ad} = -T \frac{\Delta S_m}{C_m} \quad (9)$$

The magnetocaloric effect is measured by a parameter called Relative Cooling Power (RCP), which is calculated from the magnetic entropy change vs temperature curves. The formula for determining of RCP is given by,

$$RCP = \int_{T_1}^{T_2} \Delta S_m(T) dT \quad (10)$$

Where, T_1 and T_2 are the cold and hot temperature corresponding the both ends of half maximum value of ΔS_m vs T curves.

3. Results and Discussions

3.1. Electronic Properties

The electronic density of states (DOS) and band structures have been calculated after optimizing the crystal structure of Al-doped YCrO₃. The band structures and DOS of YAl_{1-x}Cr_xO₃ ($x = 0.1$ and 0.3) have been shown in figure 2. Spin-polarized GGA+U method has been applied to determine the energy band of these systems. Figure 2(a) and 2(c) represent the band structure, which has been calculated along with the high symmetry points in Brillouin zone for the majority (UP) and minority (DOWN) spin direction, of YAl_{0.1}Cr_{0.9}O₃ and YAl_{0.3}Cr_{0.7}O₃ respectively. The dotted line corresponds the Fermi energy (E_F), which separates the valance band and conduction band of Al-doped YCrO₃. The majority spin band gaps at Γ points (direct bandgap, $\Gamma \rightarrow \Gamma$) are 2.55 eV and 2.5 eV for 10% and 30% Al-doped samples. The UP spin direct bandgap for YCrO₃ is 2.61 eV, which means the bandgap is decreasing with increasing Al concentration. The experimental band gap of YCO₃ is reported to 1.86 and 2.86 eV [37], which is nearly same as our theoretical value 1.90 eV and 2.61 eV. The minority spins have shown the indirect bandgap ($Z \rightarrow \Gamma$) which are 1.9 eV, 1.95 eV, 1.951 eV and 2.08 eV respectively for $x = 0.0, 0.1, 0.3, 0.5$ doping concentrations.

To study more intensely about the energy states below and above the Fermi level, we have calculated the partial DOS (PDOS) of Y-d, Cr-d, Al-p and O-p states. The total DOS and PDOS have been described in figure 2(b), and 2(d) for YAl_{0.1}Cr_{0.9}O₃ and YAl_{0.3}Cr_{0.7}O₃, respectively. The conduction band mainly consists of Y-d states as well as Cr-d

states. The spin up and down channel, the minima of the conduction band at Γ and X point originated due to the Cr-d states. O-p states are responsible for the valance band maxima in the spin-down channel at Z point. The Al-p, O-s states are responsible for lower band below -8 eV. The asymmetry in the up and down spin channel for Cr-d states confirms that it is ferromagnetic in nature.

3.2. Magnetic Properties

The ground state magnetic properties of Al-doped YCrO₃ compounds have been studied using the spin polarization GGA-PBE+U method. These systems are optimized with two different magnetic spin systems of the magnetic Cr-atom. The interaction between two nearest neighbours Cr-atom is considered to be a ferromagnetic (FM) and antiferromagnetic (AFM), respectively. It is seen that the energy eigenvalues of the FM configuration are less than the AFM for all cases. So, the ground state spin structure of these compounds are ferromagnetic. The magnetic moments per Cr atom for FM configuration are 1.5 μ_B , 1.31 μ_B , 1.13 μ_B , 0.75 μ_B for YAl_xCr_{1-x}O₃, (where $x = 0.0, 0.1, 0.3, 0.5$) respectively.

Figure 3(a) represents the magnetization per Cr-atom of YAl_xCr_{1-x}O₃, (where $x = 0.0, 0.1, 0.3, 0.5$) as a function of temperature without any external magnetic field. The paramagnetic transition temperature (T_C) decreases with increasing Al doping concentrations. To determine the exact transition temperature, we have differentiated the magnetization with respect to temperature and plotted the obtained $\frac{dM}{dT}$ curve with temperature (T) in figure 3(b). The minimum point of this curve indicates the magnetic ordering temperatures at 136 K, 126 K, 110 K and 73 K for YAl_xCr_{1-x}O₃ compound with $x = 0.0, 0.1, 0.3$ and 0.5 respectively. The obtained values of transition temperature are comparable to the experimental results. The saturation magnetization (M_S) decreases linearly with this equation, $M_S = M_{S_0}(1 - x)$, where M_{S_0} is the saturation magnetization of starting material YCO and x is the different Al concentrations. The temperature-dependent magnetic susceptibility and specific heat are shown in figure 3(c) and 3(d) for different Al doping concentrations. These two observables are calculated from the magnetic and energy fluctuation, respectively, with the help of equation (5) and (6). The peaks in these two figures signify the transition temperature of these materials, which is as same as calculated earlier.

Figure 4(a) shows the temperature dependence of magnetization in the presence of the different applied external magnetic field, where the steepness of the curve depends on the applied magnetic field. It is seen that the saturation magnetization is the same for all applied field, but the transition temperature shifts towards the higher values for increasing of the applied field. The increase in T_C indicates that the external magnetic field influences the magnetic interaction between two nearest neighbour magnetic ion. The alignment of all spins of Cr³⁺ ion becomes uni-direction, i.e. towards the external field direction before the transition temperature upon cooling of this material. The ground state magnetic

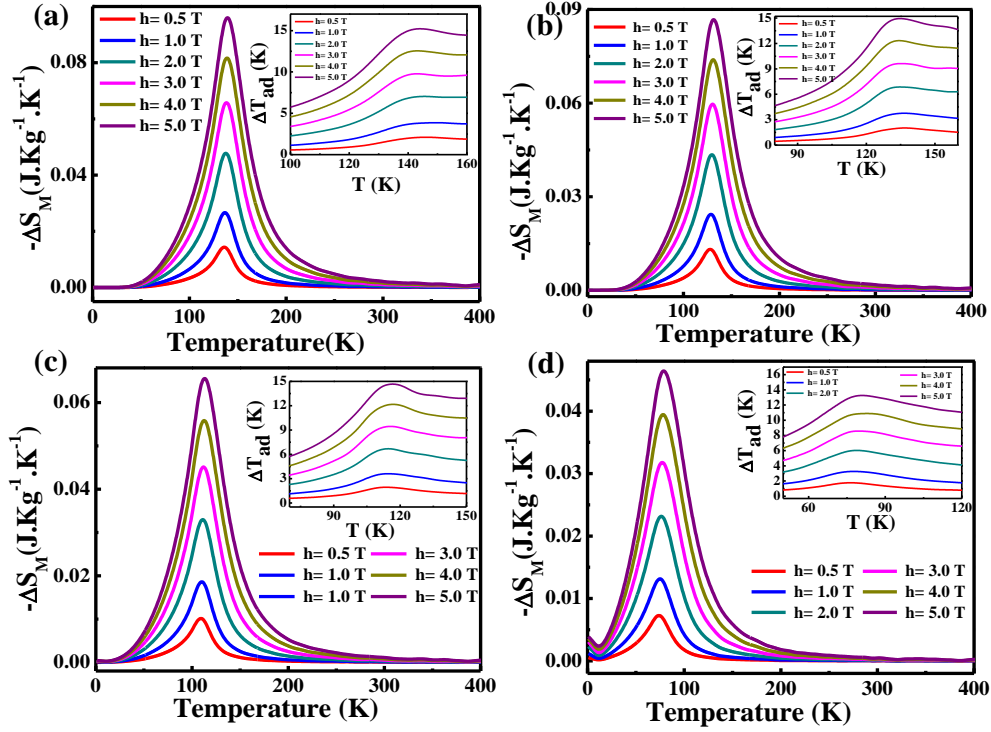


Figure 5: Negative magnetic entropy changes with respect to temperature and the inset shows the temperature dependence of adiabatic temperature change for $\text{YCr}_{1-x}\text{Al}_x\text{O}_3$ with different external magnetic field (a) $x = 0.0$, (b) $x = 0.1$, (c) $x = 0.3$ (d) $x = 0.5$

energy per spin is shown in figure 4(b). The ground state magnetic energy is calculated from mean-field theory using the relation $E_0 = -\frac{1}{2}Z_{eff}J_{eff}S_{eff}^2$ [38]. The values of ground-state free energy are -86.94 meV, -76.71 meV, -53.01 meV and -28.84 meV for $x=0, 0.1, 0.3$ and 0.5 respectively. From our simulation, we have seen the values of free energies are -85.89 meV, -76.08 meV, -52.78 meV and -28.82 meV respectively, which is very similar to the calculated values. The big change of slope in the curves indicates the phase transitions temperature of these materials. Figure 4(c) and (d) show how the magnetization changes with the applied magnetic field from 50 T to -50 T at 20 K and 200 K respectively. From 20 K hysteresis loop, we see that the remnant magnetization as well as the coercive field both decreases with increasing Al concentrations. The Al doping also causes the reduction of the saturation magnetization (M_S) below the transition temperature. Below the transition temperature, it shows the wide gap between negative and positive values of the applied field, which confirms the ferromagnetic nature of these materials. Above the transition temperature, they have not shown any remnant magnetization as well as the coercive field. This type of behaviour supports the paramagnetic nature of these materials.

3.3. Magnetocaloric Effect

The magnetic entropy change ($-\Delta S_m$) with respect to temperature for different applied magnetic field has been shown in figure 5(a-d) for $\text{YAl}_x\text{Cr}_{1-x}\text{O}_3$, $x = 0.0, 0.1, 0.3$ and 0.5 . The symmetric peak of these curves indicates the second-

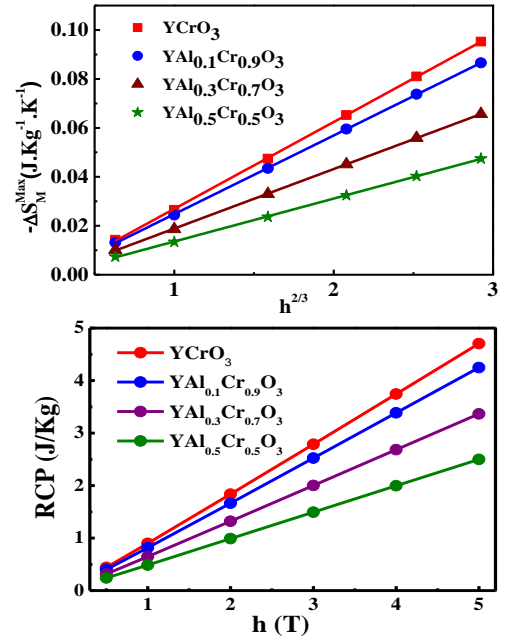


Figure 6: (a) Maximum entropy change with respect to the two third of the external magnetic field. (b) RCP versus external magnetic field for different materials.

order phase transition. It shows the positive value over the all temperature range around the wide range of the transition temperature, which is very useful for magnetic refrigeration

around 136 K, 126 K, 110 K and 73 K. For an active regenerative magnetic refrigerator, we need a series of different T_C materials. So, we have doped the non-magnetic Al in different composition in the Cr site to reduce transition temperature gradually towards the lowering temperature. The magnitude, as well as the full-width at the half maximum (FWHM) of the curve, is gradually increasing with the applied field. The value of FWHM (ΔT) is a very useful parameter to determine the operating temperature range of the magnetic refrigeration. In our case the value of FWHM of 5 tesla external field is 49.39 K, 49.07 K, 51.23 K and 52.66 K for $YAl_xCr_{1-x}O_3$, $x = 0.0, 0.1, 0.3$ and 0.5 respectively. The maximum value of $-\Delta S_m$ as a function of two-third power of applied field ($h^{2/3}$) increases linearly, which indicates again that it is the second-order phase transition, shown in figure 6(a).

The adiabatic temperature change (ΔT) in the presence of the magnetic field has been calculated from magnetic entropy difference and magnetic specific heat. The inset of figure 5(a-d) is described this adiabatic temperature change, which is maximum at the transition temperature. The values of ΔT_{max} which is proportional to the applied magnetic field are 15.3 K, 15 K, 14.6 K and 13.3 K of 5 T magnetic field for $YAl_xCr_{1-x}O_3$, $x = 0.0, 0.1, 0.3$ and 0.5 respectively. This is a very useful parameter which describes the amount of cooling performance of the material. The value tells us that it is very effective as magneto-caloric refrigerator applications.

Finally, we have measured the relative cooling power (RCP) of these set of materials as a function of the applied magnetic field. This parameter plays a vital role to characterise the magneto-caloric material as well as to determine the efficiency of magnetic cooling. The RCP value, which is shown in figure 6(b), increases linearly with increasing applied field. The RCP decreases with increasing Al concentrations.

4. Conclusions

In this current paper, we have studied electronic and magnetic properties of aluminium doped yttrium chromate using first principle calculations after that we have re-investigated the magnetic properties and studied the magneto-caloric effect of these systems using Monte- Carlo simulations. We have seen that the bandgap of these materials are indirect due to the valance band maxima (Z- point) and conduction band minima Γ point are different point of symmetry in the Brillouin boundary. The calculated magnetic moment of Cr atom from ab-initio study and Monte-Carlo simulations at ground state is the same one. The ferromagnetic transition temperature (T_C) of these materials decreases with increasing Al- concentrations and simulated T_C is as same as the experimental value. The magnetic entropy change (ΔS_m) and adiabatic temperature change (ΔT) have been calculated to study the magneto-caloric effect of these materials. The RCP value increases linearly with the application of the higher external magnetic field. We propose that we can easily reach into the liquid nitrogen temperature (78 K) using these series of Al-doped $YCrO_3$ as the magnetic ele-

ments of a magnetic refrigerator.

5. Acknowledgement

T.K Bhowmik would like to thank Department of Science and Technology (DST), Government of India for providing the financial support in the form of DST-INSPIRE fellowship (IF160418).

References

- [1] H. Das, U. V. Waghmare, T. Saha-Dasgupta, D. D. Sarma, Electronic structure, phonons, and dielectric anomaly in ferromagnetic insulating double perovskite La_2NiMnO_6 , *Phys. Rev. Lett.* 100 (2008) 186402.
- [2] S. Baidya, T. Saha-Dasgupta, Electronic structure and phonons in La_2CoMnO_6 : A ferromagnetic insulator driven by coulomb-assisted spin-orbit coupling, *Phys. Rev. B* 84 (2011) 035131.
- [3] B. Kim, J. Lee, B. H. Kim, H. C. Choi, K. Kim, J.-S. Kang, B. I. Min, Electronic structures and magnetic properties of a ferromagnetic insulator: La_2MnNiO_6 , *Journal of Applied Physics* 105 (2009) 07E515.
- [4] W. Yi, Y. Matsushita, A. Sato, K. Kosuda, M. Yoshitake, A. A. Belik, $Bi_3Cr_{2.91}O_{11}$: A ferromagnetic insulator from cr^{4+}/cr^{5+} mixing, *Inorganic Chemistry* 53 (2014) 8362–8366. PMID: 25089932.
- [5] N. Rogado, J. Li, A. Sleight, M. Subramanian, Magnetocapacitance and magnetoresistance near room temperature in a ferromagnetic semiconductor: La_2NiMnO_6 , *Advanced Materials* 17 (2005) 2225–2227.
- [6] W. Chen, J. George, J. B. Varley, G.-M. Rignanese, G. Hautier, High-throughput computational discovery of $In_2Mn_2O_7$ as a high curie temperature ferromagnetic semiconductor for spintronics, *npj Computational Materials* 5 (2019) 72.
- [7] T. Xiao, G. Wang, Y. Liao, Theoretical prediction of a two-dimensional intrinsic double-metal ferromagnetic semiconductor $MnCoO_4$, *Applied Surface Science* 450 (2018) 422 – 428.
- [8] X. Tan, E. E. McCabe, F. Orlandi, P. Manuel, M. Batuk, J. Hadermann, Z. Deng, C. Jin, I. Nowik, R. Herber, C. U. Segre, S. Liu, M. Croft, C.-J. Kang, S. Lapidus, C. E. Frank, H. Padmanabhan, V. Gopalan, M. Wu, M.-R. Li, G. Kotliar, D. Walker, M. Greenblatt, $MnFe_{0.5}Ru_{0.5}O_3$: an above-room-temperature antiferromagnetic semiconductor, *J. Mater. Chem. C* 7 (2019) 509–522.
- [9] T. Goto, T. Kimura, G. Lawes, A. P. Ramirez, Y. Tokura, Ferroelectricity and giant magnetocapacitance in perovskite rare-earth manganites, *Phys. Rev. Lett.* 92 (2004) 257201.
- [10] S. Mori, J. Tokunaga, Y. Horibe, Y. Aikawa, T. Katsufuji, Magnetocapacitance effect and related microstructure in Ti-doped $YMnO_3$, *Phys. Rev. B* 72 (2005) 224434.
- [11] M. P. Singh, K. D. Truong, P. Fournier, Magnetodielectric effect in double perovskite La_2CoMnO_6 thin films, *Applied Physics Letters* 91 (2007) 042504.
- [12] R. P. Maiti, S. Dutta, M. K. Mitra, D. Chakravorty, Large magnetodielectric effect in nanocrystalline double perovskite Y_2FeCrO_6 , *Journal of Physics D: Applied Physics* 46 (2013) 415303.
- [13] S. B. Kim, Y. H. Park, H. jun Kim, J. Chang, H. C. Koo, Magnetoresistance of a ferromagnet/semiconductor interface with a strong rashba effect, *Thin Solid Films* (2020) 138047.
- [14] S. Yamada, N. Abe, H. Sagayama, K. Ogawa, T. Yamagami, T. Arima, Room-temperature low-field colossal magnetoresistance in double-perovskite manganite, *Phys. Rev. Lett.* 123 (2019) 126602.
- [15] S. Roy, N. Khan, P. Mandal, Giant low-field magnetocaloric effect in single-crystalline $EuTi_{0.85}Nb_{0.15}O_3$, *APL Materials* 4 (2016) 026102.
- [16] S. Pakhira, C. Mazumdar, R. Ranganathan, M. Avdeev, Magnetic frustration induced large magnetocaloric effect in the absence of long range magnetic order, *Scientific Reports* 7 (2017) 7367.
- [17] S.-J. Chang, M.-H. Chung, M.-Y. Kao, S.-F. Lee, Y.-H. Yu, C.-C. Kaun, T. Nakamura, N. Sasabe, S.-J. Chu, Y.-C. Tseng, $GdFe_{0.8}Ni_{0.2}O_3$: A multiferroic material for low-power spintronic de-

- vices with high storage capacity, *ACS Applied Materials & Interfaces* 11 (2019) 31562–31572.
- [18] Y. Fu, H. Zhu, J. Chen, M. P. Hautzinger, X.-Y. Zhu, S. Jin, Metal halide perovskite nanostructures for optoelectronic applications and the study of physical properties, *Nature Reviews Materials* 4 (2019) 169–188.
- [19] Y.-M. You, W.-Q. Liao, D. Zhao, H.-Y. Ye, Y. Zhang, Q. Zhou, X. Niu, J. Wang, P.-F. Li, D.-W. Fu, Z. Wang, S. Gao, K. Yang, J.-M. Liu, J. Li, Y. Yan, R.-G. Xiong, An organic-inorganic perovskite ferroelectric with large piezoelectric response, *Science* 357 (2017) 306–309.
- [20] M. Foldeaki, R. Chahine, T. K. Bose, Magnetic measurements: A powerful tool in magnetic refrigerator design, *Journal of Applied Physics* 77 (1995) 3528–3537.
- [21] W. Gifford, Refrigeration to below 20 k, *Cryogenics* 10 (1970) 23 – 27.
- [22] R. Mascheroni, V. Salvadori, Household Refrigerators and Freezers, pp. 253–272.
- [23] N. Mezaal, K. Osintsev, T. Zhirgalova, Review of magnetic refrigeration system as alternative to conventional refrigeration system, *IOP Conference Series: Earth and Environmental Science* 87 (2017) 032024.
- [24] W. Kohn, L. J. Sham, Self-consistent equations including exchange and correlation effects, *Phys. Rev.* 140 (1965) A1133–A1138.
- [25] J. P. Perdew, K. Burke, M. Ernzerhof, Generalized gradient approximation made simple, *Phys. Rev. Lett.* 77 (1996) 3865–3868.
- [26] V. I. Anisimov, F. Aryasetiawan, A. I. Lichtenstein, First-principles calculations of the electronic structure and spectra of strongly correlated systems: the LDA+U method, *Journal of Physics: Condensed Matter* 9 (1997) 767–808.
- [27] Toulouse, G., Gabay, M., Mean field theory for heisenberg spin glasses, *J. Physique Lett.* 42 (1981) 103–106.
- [28] C. Holm, W. Janke, Critical exponents of the classical three-dimensional heisenberg model: A single-cluster monte carlo study, *Physical Review B* 48 (1993) 936–950.
- [29] A. L. Talapov, H. W. J. Blote, The magnetization of the 3D Ising model, *Journal of Physics A: Mathematical and General* 29 (1996) 5727–5733.
- [30] K. Binder, D. Heermann, L. Roelofs, A. J. Mallinckrodt, S. McKay, Monte carlo simulation in statistical physics, *Computers in Physics* 7 (1993) 156–157.
- [31] A. N. Jara, J. F. Carvalho, A. F. Junior, L. J. Maia, R. C. Santana, On the optical and magnetic studies of YCrO_3 perovskites, *Physica B: Condensed Matter* 546 (2018) 67 – 72.
- [32] A. DurÅan, E. VerdÅnn, A. Conde, R. Escamilla, Effect of Al-doped YCrO_3 on structural, electronic and magnetic properties, *Journal of Magnetism and Magnetic Materials* 453 (2018) 36 – 43.
- [33] Y. Aray, J. Rodriguez, D. Vega, An implementation of the atoms in molecules theory to the fplapw method, *Computer Physics Communications* 143 (2002) 199 – 212.
- [34] P. Blaha, K. Schwarz, P. Sorantin, S. Trickey, Full-potential, linearized augmented plane wave programs for crystalline systems, *Computer Physics Communications* 59 (1990) 399 – 415.
- [35] P. Blaha, K. Schwarz, F. Tran, R. Laskowski, G. K. H. Madsen, L. D. Marks, Wien2k: An apw+lo program for calculating the properties of solids, *The Journal of Chemical Physics* 152 (2020) 074101.
- [36] J. H. Van Vleck, On the theory of antiferromagnetism, *The Journal of Chemical Physics* 9 (1941) 85–90.
- [37] P. Saxena, D. Varshney, Structural and electrical properties of Sr doped YCrO_3 , *AIP Conference Proceedings* 1942 (2018) 110040.
- [38] H. T. Diep, *Theory of Magnetism*, WORLD SCIENTIFIC, 2014.